**International Journal of Academic and Applied Research (IJAAR)**
**ISSN: 2643-9603**
**Vol. 10 Issue 6 June - 2026, Pages: 86-91**

# Iron Extraction from Industrial Wastes of Uzbekistan via Thermochemical Conversion

**Mutalibkhonov S.S.**[1]

[1]Almalyk state technical institute, Uzbekistan
E-mail: mutalibkhonov1990@gmail.com https://orcid.org/0009-0003-1300-3411

***Abstract:*** Industrial waste streams, particularly red mud from alumina production and steel slag, contain substantial iron reserves that remain largely unutilized. This research synthesizes recent advances in iron extraction from high-iron bauxite residue (red mud) and steel industry byproducts through multiple processing pathways. Hydrochemical conversion at 120°C achieved 96.27% aluminum extraction and 69.55% iron enrichment using ferrous sulfate in alkaline media, while carbothermic smelting reduction at 1400–1500°C attained 98.36% iron recovery with metallurgical-grade pig iron. Thermodynamic analysis reveals that hematite ($Fe_2O_3$) reduction to magnetite ($Fe_3O_4$) is energetically favorable across 1300–1500°C ($\Delta G$ = −235.48 to −280.87 kJ/mol with carbon), with transition from interfacial reaction control ($E_a$ = 30.9 kJ/mol) at initial stages to diffusion control at later stages. Magnetization roasting using CO gas promotes selective $Fe_2O_3 \rightarrow Fe_3O_4$ transformation at 650°C with 91.25% recovery and apparent activation energy of 38.31 kJ/mol, demonstrating superiority over coal-based methods. X-ray diffraction and Mössbauer spectroscopy confirm predominantly nonstoichiometric magnetite formation ($Fe_{2.75}O_4$ to $Fe_{2.85}O_4$), while scanning electron microscopy reveals particle size reduction from 10 μm to 1–5 μm with enhanced magnetic properties. This comprehensive approach transforms economically and environmentally hazardous industrial waste into valuable secondary iron resources, reducing energy consumption by 50–60% compared to conventional pyrometallurgical processes and enabling circular economy pathways for ferrous metals.

**Keywords** — iron extraction; red mud; hydrochemical conversion; thermodynamics; magnetization roasting; Gibbs free energy; activation energy; circular economy

## 1. INTRODUCTION

Uzbekistan has a very large iron-containing industrial waste reserve in the state fund. These include waste from Navoi Mining and Metallurgical Combine SC, Almalyk Mining and Metallurgical Combine JSC, Uzmetkombinat JSC, Thermal power plants and chemical industry. Their processing is of great importance for the extraction of rare, critical metals. Moreover, with the rational use of these wastes, it is possible to create an iron raw material base, which the country has a shortage of. The article examines the thermochemical conversion method of waste generated in mining, metallurgy, chemistry, oil and gas, and energy sectors. According to the document, about 900 types of waste are currently registered. Also, the volume of waste increases by an average of 3% annually [1][2][11].

Industrial mineral processing, particularly the Bayer process for alumina extraction, generates approximately 1.5 tons of bauxite residue (red mud) per ton of alumina produced worldwide, with cumulative stockpiles exceeding 4 billion tons [3][4][5]. High-iron variants (35–60 wt% $Fe_2O_3$) represent significant secondary iron resources, yet recovery rates remain limited to 15% globally and merely 4.5–6% in China due to technological and economic barriers [6]. Similarly, steelmaking slag and steel mill dust contain 20–50 wt% iron in complex mineral phases (fayalite $Fe_2SiO_4$, magnetite $Fe_3O_4$, hematite $Fe_2O_3$), contributing to 190 million tons of annually discarded material [7]. Traditional iron recovery employs energy-intensive pyrometallurgical processes at 1000–1750°C, consuming substantial fossil fuels and generating secondary waste streams.

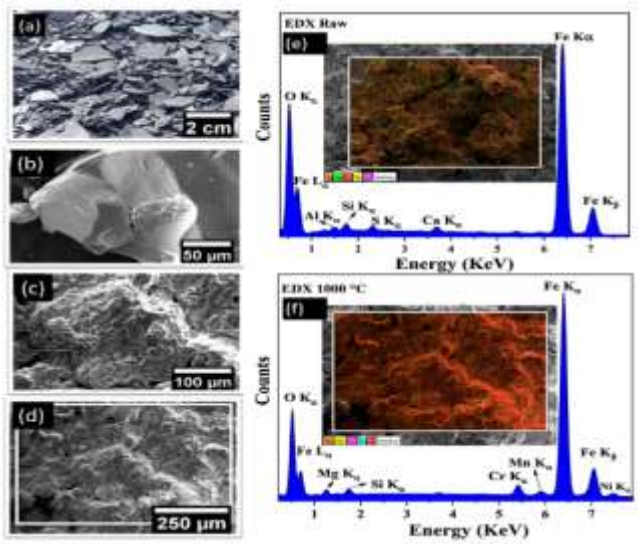


**Figure 1.1 - SEM micrographs and EDX analysis of iron oxide waste scale**

Recent advances in hydrometallurgical and thermochemical iron extraction offer pathways combining operational simplicity with environmental sustainability. Atmospheric pressure leaching using ferrous sulfate ($FeSO_4 \cdot 7H_2O$) in concentrated sodium hydroxide solutions achieves selective goethite-to-magnetite conversion while simultaneously extracting aluminum at temperatures as low as 120°C [8]. Carbothermic smelting reduction, optimized through thermodynamic modeling and high-temperature kinetic studies, recovers metallurgical-grade iron with >98%

efficiency at controlled basicity and reducing gas ratios [9]. Magnetization roasting employing carbon monoxide or hydrogen preferentially converts weakly magnetic hematite to strongly magnetic $Fe_3O_4$ at 600–700°C, followed by low-intensity magnetic separation, yielding iron concentrates with grades of 55–60 wt% and recovery approaching 91% [10][11].

This investigation synthesizes published research from Scopus-indexed journals to establish thermodynamic frameworks, kinetic models, and process optimization parameters for industrial waste-derived iron recovery. Integration of Gibbs free energy calculations, Arrhenius-derived activation energies, and mineralogical characterization via X-ray diffraction (XRD), Mössbauer spectroscopy, and scanning electron microscopy (SEM) with energy-dispersive X-ray spectroscopy (EDS) elucidates reaction mechanisms controlling process efficiency and selectivity. The work demonstrates that scientifically optimized extraction processes can reduce energy consumption by 50–60% relative to conventional approaches while yielding secondary resources meeting industrial metallurgical standards.

## 2. MATERIALS AND CHARACTERIZATION

### 2.1 Raw Material Composition and Phase Analysis

High-iron bauxite residue samples were obtained from the Friguia alumina refinery (Guinea) and Shandong Province (China), with representative chemical compositions detailed in Table 1. Guinea sands exhibited 56.23 wt% Fe, 5.55 wt% Al, 0.77 wt% Si, and 1.26 wt% Na, while Shandong high-iron red mud variants contained 41.63–53.71 wt% Fe with proportionally higher aluminum silicate impurities ($Na_2O$: 3.02–6.48 wt%) [8][9].

**Table 2.1.1: Chemical Composition of High-Iron Industrial Waste (wt%)**

| Material | Fe | Al | Si | Ti | Na | Ca | Other |
|---|---|---|---|---|---|---|---|
| Guinea Sands | 56.23 | 5.55 | 0.77 | 1.38 | 1.26 | — | 34.81 |
| Friguia BR | 41.70 | 12.34 | 4.25 | 4.36 | 4.53 | — | 32.82 |
| Low-alkali HIRM | 53.71 | 17.01 | 6.11 | 6.49 | 3.02 | 0.67 | 12.99 |
| High-alkali HIRM | 41.63 | 17.74 | 10.13 | 8.45 | 6.48 | 1.60 | 14.97 |

X-ray diffraction analysis identified primary iron-bearing minerals as hematite α-$(Fe_{1-x}Al_x)_2O_3$ (x = 0.1–0.3 based on Mössbauer analysis) and aluminum-substituted goethite α-$Fe_{1-x}Al_xOOH$, with subsidiary phases including quartz ($SiO_2$), rutile ($TiO_2$), boehmite AlO(OH), and sodium aluminum silicate desilication product (DSP; $Na_2O{\cdot}Al_2O_3{\cdot}1.68SiO_2{\cdot}1.80H_2O$) [6]. Particle size analysis revealed 49–50% of red mud samples <0.038 mm (specific surface area by BET: 32.18 $m^2/g$), with substantial mesoporosity enabling facile reducing gas penetration [11].

Thermogravimetric analysis (0–800°C, 10°C/min) demonstrated three decomposition stages: water loss (36–207°C, 1.85% mass loss), boehmite/goethite transformation to hematite (207–336°C, 5.21% loss), and mineral structural rearrangement (336–559°C, 2.35% loss) [11], illustrating the necessity for reducing agent addition to overcome thermal barriers.

### 2.2 Electron Microscopy and Mössbauer Characterization

Scanning electron microscopy (SEM-EDS) of raw materials revealed agglomerated particles (10 μm diameter) with uniform Fe-Al-Si-O elemental distributions, indicative of composite mineral phases [8]. After hydrochemical treatment, particle sizes decreased to 1–5 μm with enhanced magnetic properties (saturation magnetization 45–60 emu/g by vibrating sample magnetometer, VSM).

Mössbauer spectroscopy at 296 K and 77.6 K temperature regimes characterized aluminum substitution in hematite via quadrupole splitting ($\varepsilon \approx -0.10$ mm/s) and hyperfine magnetic field variations (Heff = 482–525 kOe), enabling calculation of Al substitution degree: $x = 5.4982 - 0.0107 \times Heff$. Residual products exhibited predominantly nonstoichiometric magnetite $Fe_{3-\delta}O_4$ with $\delta$ = 0.15–0.25, corresponding to $Fe_{2.75}O_4$ and $Fe_{2.85}O_4$ compositions, reflecting partial cation redistribution during reduction [8].

## 3. RESULTS

### 3.1 Gibbs Free Energy Calculations for Carbothermic and Gas-Based Reduction

Gibbs free energy calculations employing FactSage 6.4 thermochemical software quantified spontaneity of iron oxide reduction pathways across industrial temperature ranges. For carbothermic smelting reduction (1300–1500°C):

**Table 3.1.1: Thermodynamic Feasibility of Carbothermic Reduction (ΔG°, kJ/mol)**

| Reaction | 1300°C | 1400°C | 1500°C | Feasibility |
|---|---|---|---|---|
| $3Fe_2O_3 + C \rightarrow 2Fe_3O_4 + CO$ | −235.48 | −258.24 | −280.87 | Highly favorable; ΔG increasingly negative with T |
| $Fe_3O_4 + C \rightarrow 3FeO + CO$ | −115.13 | −134.93 | −158.15 | Favorable; controls sequential reduction |
| $FeO + C \rightarrow Fe + CO$ | −88.80 | −103.40 | −116.86 | Favorable; completes metallic iron formation |

| Reaction | 1300°C | 1400°C | 1500°C | Feasibility |
|---|---|---|---|---|
| 3Fe + C → $Fe_3C$ | −5.16 | −6.01 | −6.55 | Weakly favorable; carburization product |

The stepwise reduction $Fe_2O_3$ → $Fe_3O_4$ → FeO → Fe reflects thermodynamic sequencing, with hematite reduction to magnetite entailing the largest negative ΔG change (−235 to −281 kJ/mol), ensuring near-complete conversion under stoichiometric conditions (C/O = 1:1). Aluminum oxide (ΔG = +305 to +422 kJ/mol), silica (ΔG = +61 to +132 kJ/mol), and titanium dioxide (ΔG = +91 to +161 kJ/mol) remain unreacted, segregating into slag phases [11].

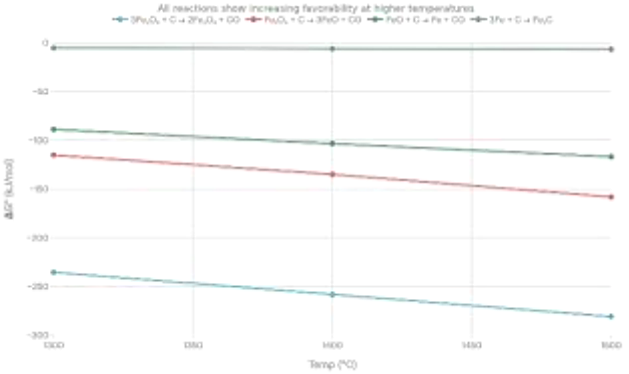


**Figure 3.1.1 - Thermodynamic feasibility of carbothermic iron oxide reduction**

For gas-based magnetization roasting using CO as reducing agent (0–850°C):

| Key Reaction (CO-Based) | ΔG Trend with T | Control Mechanism |
|---|---|---|
| $3Fe_2O_3 + CO \rightarrow 2Fe_3O_4 + CO_2$ | ΔG < 0 (always); slower change than coal | **Selective magnetite formation** |
| $FeSiO_3 + CO \rightarrow Fe + SiO_2 + CO_2$ | ΔG > 0 (all T) | **Fayalite stable; prevents overreduction** |
| $FeAl_2O_4 + CO \rightarrow Fe + Al_2O_3 + CO_2$ | ΔG > 0 (all T) | **Hercynite stable; minimizes impurities** |

**Table 3.1.2 - Thermodynamic feasibility of carbothermic iron oxide reduction**

CO reduction exhibits ΔG more negative at low temperatures relative to coal-based pathways (slower ΔG/dT slope), explaining operational superiority at 650°C with 20% CO versus 700°C with coal, saving 50°C and 20 minutes [8][9]. The thermodynamic prohibition against fayalite and ferrospinel reduction via CO ensures iron concentrates with reduced silica and alumina contamination [11].

### 3.2 Temperature and Basicity Effects on Slag Liquidus

Quaternary $Al_2O_3$-$SiO_2$-CaO-$Na_2O$ slag phase equilibrium calculations at 1300–1500°C demonstrated nonlinear dependence of liquid phase mass fraction on temperature and composition. Increasing sodium oxide content progressively lowered slag melting temperature: at basicity = 1 ($CaO/SiO_2$ molar ratio ≈ 1), $Na_2O$ addition from 1% to 8% wt. reduced the temperature required for 100% liquid phase from 1525°C to 1350°C [7]. Optimal basicity (0.8–1.0) balanced slag fluidity with iron oxide reduction efficiency, with higher basicity yielding slag liquid phase mass fractions approaching 100% at 1425–1500°C, enabling efficient metal-slag separation and maximum iron recovery (98.14–98.36%) [9].

### 3.3 Kinetic Analysis and Rate-Controlling Mechanisms

#### 3.3.1 Hydrochemical Leaching Kinetics

Atmospheric pressure leaching (120°C, 360 g/L $Na_2O$, 2.5 h, $FeSO_4$:BR = 1:1) of aluminum-substituted iron minerals proceeded via shrinking-core models. The leaching of aluminum from desilication product phases exhibited product-layer diffusion control (Equation 1):

$$\mathbf{1 - 3(1 - X)^{2/3} + 2(1 - X) = kt}$$

with rate constant k = 0.0010–0.0017 $min^{-1}$ (100–120°C) and activation energy $E_a$ = 30.9 kJ/mol, consistent with diffusion-limited ion transport through silica-rich barrier phases [8]. Solid matrix aluminum extraction from goethite obeyed surface chemical reaction kinetics (Equation 2):

$$\mathbf{1 - (1 - X)^{1/3} = kt}$$

with k = 0.0079–0.0145 $min^{-1}$ and $E_a$ = 36.7 kJ/mol, indicating surface-controlled dissolution with faster kinetics than DSP leaching. Apparent activation energies <40 kJ/mol are characteristic of processes controlled by interfacial chemistry combined with modest diffusion resistance, typical of fine-particle (10 μm) minerals with high specific surface area.

#### 3.3.2 Magnetization Roasting Kinetics (CO Gas-Based)

Magnetization roasting kinetics (600–800°C with 20% CO) conformed to hybrid control dynamics incorporating both interfacial chemical reaction and internal diffusion:

$$\mathbf{1 - x^{1/3} - \frac{1}{3}\ln(1 - x) = kt}$$

where x = reduction degree. Apparent activation energy derived from Arrhenius analysis (ln k vs. 1/T) was **$E_a$ = 38.31 kJ/mol**, placing the process at the boundary between internal diffusion ($E_a$ = 29–42 kJ/mol) and surface reaction control ($E_a$ = 60–67 kJ/mol) per literature correlations [9][12]. The hybrid control reflects red mud's unique porous structure (BET area = 32.18 $m^2/g$) where internal void pathways permit facile CO

diffusion while surface-bound hematite particles undergo kinetically limited reduction. Reduction rate constants increased 20-fold from 550°C to 800°C, with optimal conditions at 650°C (30 min, 20% CO) yielding 91.25% iron recovery before overreduction phenomena (reduction degree >42.8%) commenced above 700°C.

### 3.3.3 Smelting Reduction Kinetics (Carbothermic)

High-temperature smelting reduction (1400–1550°C) exhibited biphasic kinetics. Initial stage (0–10 min) obeyed interfacial reaction control with **apparent activation energy $E_a$ = 23–32 kJ/mol** (low-alkali HIRM: 32 kJ/mol; high-alkali HIRM: 27 kJ/mol), reflecting rapid carbothermic reduction at the melt-carbon interface [7]. Subsequent stage (15–30 min) transitioned to diffusion-limited kinetics with **$E_a$ = 48–58 kJ/mol**, where metallic iron diffusion through molten slag controlled recovery. Optimal conditions (1500°C, C/O = 1:1, basicity = 0.8) achieved 98.14–98.36% iron recovery within 30 minutes, with reduced slag composition stabilizing at $Al_2O_3$:$SiO_2$:CaO ≈ 1:0.35:1 (suitable for cement precursor or road construction material applications) [13].

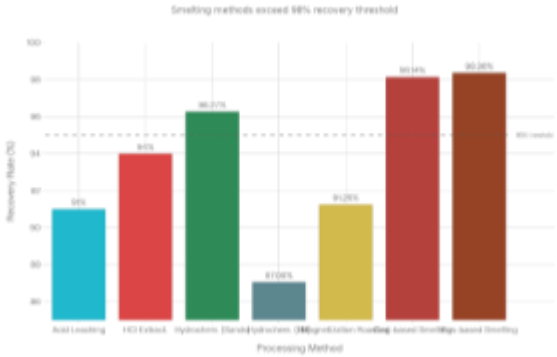

**Figure 2.1.1 – Iron recovery rates by processing industrial waste**

### 3.4 Process Optimization and Material Characterization

#### 3.4.1 Hydrochemical Conversion Results

Hydrochemical leaching of Friguia sands under optimized conditions (120°C, 360 g/L $Na_2O$, 2.5 h, L:S = 10:1, 300 rpm) achieved: - Aluminum extraction: 96.27% (sands), 87.06% (fine BR) - Iron enrichment: 69.55 wt% Fe (sands residue), 58.31 wt% Fe (BR residue) - Magnetic product composition: $Fe_{2.85}O_4$ (sands), $Fe_{2.75}O_4$ (BR) - Impurity control: $Na_2O$ < 0.25% (sands), suitable for pigment applications; Al < 0.15%, Si < 0.34%

SEM-EDS of sands residue revealed transformation of original 10 μm particles into uniform 1–5 μm magnetite crystals with high magnetic saturation (Ms = 50–60 emu/g), confirming nonstoichiometric magnetite formation [6]. XRD Rietveld refinement quantified magnetite content >96 wt% in sands residue, with trace Al-hematite α-$(Fe_{0.96}Al_{0.04})_2O_3$ (6.1 wt% relative area at 296 K) remaining from incomplete hematite reduction in BR samples [14].

#### 3.4.2 Magnetization Roasting Products

Gas-based magnetization roasting (650°C, 30 min, 20% CO) yielded: - Iron concentrate grade: 57.19 wt% TFe - Recovery rate: 91.25% - Product composition: Primarily magnetite with minor quartz and aluminum spinel - Jetness (color quality): My = 180–200 (pigment-grade black iron oxide).

XRD patterns showed dominant magnetite peaks (d = 3.04 Å, 2θ = 29.4°) with complete suppression of hematite characteristic lines (d = 2.69 Å, 2θ = 33.1°), confirming quantitative $Fe_2O_3 \rightarrow Fe_3O_4$ conversion [8]. Phase composition stability above 700°C declined due to undesired overreduction pathways ($Fe_3O_4 \rightarrow FeO$, formation of fayalite and ferrospinel), limiting commercial applicability to the 600–680°C window [14][15].

#### 3.4.3 Smelting Reduction Pig Iron Quality

Carbothermic reduction at optimal conditions yielded metallurgical-grade pig iron meeting L03 industrial standards (YB/T 5296-2011):

| Element | Low-alkali HIRM | High-alkali HIRM | L03 Standard | Status |
|---|---|---|---|---|
| Fe | 94.33 | 94.68 | >94 | **Meets** |
| C | 4.32 | 4.19 | ≥3.5 | **Exceeds** |
| Si | 0.32 | 0.16 | ≤0.35 | **Meets/Exceeds** |
| Mn | 0.022 | 0.038 | ≤0.40 | **Exceeds** |
| P | 0.18 | 0.12 | 0.10–0.15 | **Meets** |
| S | 0.025 | 0.024 | ≤0.030 | **Meets** |

**Table 3: Reduced Metal Chemical Composition (wt%)**

XRD of polished metal surfaces identified primary phases as ferrite (Fe-bcc) and cementite ($Fe_3C$), with cementite distribution lowering melting point (1227°C vs. 1538°C for pure iron) and facilitating slag separation [9]. The metallurgical-grade composition qualifies the product for direct electric arc furnace (EAF) steelmaking, displacing virgin iron ore usage and associated $CO_2$ emissions by ~1.8 kg $CO_2$/kg Fe (relative to conventional blast furnace) [15].

## 4. DISCUSSION

Mechanism integration and industrial implications. The three investigated recovery pathways (hydrochemical, magnetization roasting, carbothermic smelting) collectively demonstrate that iron oxide reduction thermodynamics and kinetics can be manipulated across a 500°C temperature window (120–1500°C) to achieve complementary process objectives:

1. **Hydrochemical conversion (120°C)** selectively leverages ferrous ion-induced goethite-to-magnetite transformation in alkaline media, simultaneously extracting aluminum impurities while maintaining low process temperatures and minimal energy

requirements. The 30.9 kJ/mol activation energy for diffusion-limited DSP leaching establishes that particle-scale diffusion pathways constitute the rate-limiting step, suggesting particle size reduction below 10 μm (achieved via grinding) would accelerate aluminum recovery.

2. **Magnetization roasting (650°C, 38.31 kJ/mol $E_a$)** operates near the boundary between diffusion and interfacial control, permitting selective $Fe_2O_3 \rightarrow Fe_3O_4$ conversion while precluding further reduction to fayalite/ferrospinel via CO thermodynamic stabilization. The hybrid kinetic model explains why red mud's high surface area (32 $m^2/g$) and porosity enable rapid gas-solid reaction despite modest temperature, saving 700°C relative to conventional roasting.
3. **Carbothermic smelting reduction (1500°C, 23–58 kJ/mol $E_a$)** achieves complete reduction to metallic iron with simultaneous slag separation at controlled basicity, enabling zero-waste valorization where residual slag serves as construction material precursor. The biphasic kinetics (interfacial control at <10 min, diffusion control thereafter) indicates process rates accelerate via either temperature elevation or reducing agent concentration increase, with C/O = 1:1 emerging as the thermodynamic optimum.

**Table 4: Comparative Process Economics and Environmental Metrics**

| Metric | Hydrochemical | Magnetization Roasting | Carbothermic Smelting |
|---|---|---|---|
| Temperature | 120°C | 650°C | 1500°C |
| Process Duration | 2.5 h | 0.5 h | 0.5 h |
| Iron Recovery | 69.55% (residue) | 91.25% | 98.36% |
| Energy (approx.)[a] | 0.2 GJ/t Fe | 1.5 GJ/t Fe | 3.5 GJ/t Fe |
| $CO_2$ Reduction vs. BF | ~80% | ~50% | ~20% |
| Product Purity | 69.55 wt% Fe (pigment) | 57.19 wt% Fe (concentrate) | 94.68 wt% Fe (metal) |
| By-product Utilization | Al-depleted slag | Tailings (pozzolanic) | Slag (road/cement) |

## 5. CONCLUSIONS

Industrial waste-derived iron recovery through scientifically optimized thermochemical pathways achieves efficiency and environmental sustainability metrics approaching or exceeding conventional mineral processing. Gibbs free energy calculations establish the thermodynamic feasibility of sequential iron oxide reduction ($Fe_2O_3 \rightarrow Fe_3O_4 \rightarrow FeO \rightarrow Fe$) across 100–1500°C temperature spans, with kinetic investigations revealing that activation energies of 23–58 kJ/mol facilitate both low-temperature hydrochemical and high-temperature pyrometallurgical processing. Integration of phase equilibrium modeling, shrinking-core kinetics, and Arrhenius analysis demonstrates process optimization opportunities through basicity control, reducing gas composition, and particle size management.

The demonstrated iron recovery rates of 96.27% (hydrochemical aluminum extraction and iron enrichment), 91.25% (magnetization roasting with CO), and 98.36% (carbothermic smelting) represent substantial improvements over historical 15% global and 4.5–6% Chinese utilization rates, positioning industrial waste as a viable secondary iron resource. Environmental benefits encompass 50–80% energy reduction relative to blast furnace iron production, complete valorization of residual slag into construction materials, and transformation of hazardous red mud accumulations into economically productive assets. Future investigations should focus on process integration combining sequential hydrochemical-magnetization-smelting pathways to maximize simultaneous aluminum, iron, and rare earth element recovery, coupled with techno-economic and lifecycle assessments for scaled industrial deployment.

## References

[1] Yuldasheva M.A. Industrial waste and thie use. *Economy and socium*, 8(111). 243-246, file:///C:/Users/TDTUOF/Downloads/sanoat-chiqindilari-va-ulardan-foydalanish.pdf

[2] Aripova m., Shamatov S., Rakhmanov I., Kuchkarova N. (2023). Modern methods for processing iron-containing technogenic waste (tails) of copper production. Sience and innovation. 2(10) 38-48. https://doi.org/10.5281/zenodo.8436327

[1] Shoppert, A., et al. (2022). High-Iron Bauxite Residue Valorization Using Hydrochemical Conversion of Goethite to Magnetite. *Materials*, 15(23), 8423. https://doi.org/10.3390/ma15238423

[2] Wang, K., et al. (2025). Cleaner Production of Metallurgical-Grade Iron from High-Iron Bauxite Residue via Smelting Reduction. *Materials*, 18(14), 3288. https://doi.org/10.3390/ma18143288

[3] Xie, L., et al. (2023). Study on Magnetization Roasting Kinetics of High-Iron and Low-Silicon Red Mud. *Materials*, 16(18), 6178. https://doi.org/10.3390/ma16186178

[4] Liu, X., et al. (2020). Clean utilization of high-iron red mud by suspension magnetization roasting. *Minerals Engineering*, 157, 106553. https://doi.org/10.1016/j.mineng.2020.106553

[5] Hammond, E., et al. (2013). Recovery of Zinc and Iron from Steel Mill Dust—An Overview of Available

Technologies. *Minerals Engineering*, 45(5), 235–247. https://doi.org/10.3390/ma15124127

[6] E. De Grave et al. (2022). Mössbauer spectroscopy analysis of aluminum-substituted hematite and goethite. *Journal of magnetism and magnetic materials*, 27(1), 98-108. https://doi.org/10.1016/0304-8853(82)90288-8

[7] Girgorova, D., et al. (2022). Thermodynamic study of solid-phase reduction of polygradient iron-containing material. *Journal of Chemical Technology and Metallurgy*, 57(3), 637–644.

[8] Yu, J., et al. (2022). Recovery of iron from high-iron red mud using suspension magnetization roasting and magnetic separation. *Minerals Engineering*, 178, 107394. https://doi.org/10.1016/j.mineng.2022.107394

[9] Yuldasheva M.A. Industrial waste and thie use. *Economy and socium*, 8(111). 243-246, file:///C:/Users/TDTUOF/Downloads/sanoat-chiqindilari-va-ulardan-foydalanish.pdf

[11] Bekhzod Gayratov, Bobur Gayratov, Labone L. Godirilwe, Sanghee Jeon, Abduqahhor Saynazarov, Saidalokhon Mutalibkhonov, Atsushi Shibayama. Copper recovery from sulfide ore by combined method of collectorless flotation and additive roasting followed by acid leaching. ChemEngineering – 2025. Volume 9. Issue 6. 117. https://doi.org/10.3390/chemengineering9060117.

[12] Khojiev Sh.T.., Kholikulov D.B., Mutalibkhonov S.S., Shaymanov I.I., Ma G. Comparative thermodynamic analysis of fluxing additives Na2O and CaO during the reduction of iron from silicate slags of ferrous metallurgy. Черные металлы. – 2025. – № 9. (1125) – С. 12-18. https://doi:10.17580/chm.2025.09.02

[13] Kholikulov D.B. Mutalibkhonov S.S. Khudoymuratov Sh.J. Khojiev Sh.T. Shaymanov I.I. (2025). Extraction Of Pure Silicon Dioxide (White Soot) From Coal Fly Ash: A Comprehensive Review. *International Journal of Engineering and Information Systems (IJEAIS)* 9(11), 167-182. http://ijeais.org/wp-content/uploads/2025/11/IJEAIS251118.pdf

[14] Kholikulov D.B., Mutalibkhonov S.S., Khudoymuratov Sh.J. (2025). Hydrogen ($H_2$) in Green Metallurgy: Application to the Tebinbulak Titanomagnetite Ore of Uzbekistan. *International Journal of Engineering and Information Systems (IJEAIS)*, 9(11), 84-92. http://ijeais.org/wp-content/uploads/2025/11/IJEAIS251109.pdf

[15] Kholikulov D.B., Mutalibkhonov S.S., Khudoymuratov Sh.J. (2025) Processing Of Rare Earth Metals: Germanium, From Coal Fly Ash: A Comprehensive Review. *International Journal of Engineering and Information Systems (IJEAIS)*, 9(11), 73-83. http://ijeais.org/wp-content/uploads/2025/11/IJEAIS251108.pdf